Organic Electronics 13 (2012) 533–540

Contents lists available at SciVerse ScienceDirect

Organic Electronics

journal homepage: www.elsevier.com/locate/orgel

# Transparent and flexible organic field-effect transistor for multi-modal sensing

Tran Quang Trung [a], Nguyen Thanh Tien [a], Young Gug Seol [a], Nae-Eung Lee [a,b,*]

[a] School of Advanced Materials Science and Engineering, Sungkyunkwan University (SKKU), Suwon, Kyunggi 440-746, Republic of Korea
[b] SKKU Advanced Institute of Nanotechnology (SAINT), and Samsung Advanced Institute for Health Sciences and Technology (SAIHST), Sungkyunkwan University (SKKU), Suwon, Kyunggi 440-746, Republic of Korea

ARTICLE INFO

*Article history:*
Received 19 November 2011
Accepted 31 December 2011
Available online 16 January 2012

*Keywords:*
Transparent
Flexible
OFET
Sensor
Multi-modal

ABSTRACT

Multi-functional devices having responsiveness to multiple physical stimuli, mechanical flexibility and optical transparency are of great interest in applications for human–machine interfaces. Here we demonstrate transparent and flexible organic field effect transistor (tf-OFET) devices with multi-modal sensing capability of detecting infrared (IR) light, pressure, and strain simultaneously. The multi-modal sensing layer with piezoelectricity and pyroelectricity was directly integrated into OFETs as the gate dielectric so that a new type of multi-modal sensing device with simple structure having possibility of increasing the sensor cell density can be easily fabricated. For decoupling of pyro- and piezoelectric responses in a single device under simultaneous stimulations of IR exposure and strain, an approach of determining two input stimuli by separating the polarization changes inside the gate dielectric ($V_o$) and the modulation in the product of effective field-effect channel mobility and gate capacitance ($\mu C$). The high sensitivity of the devices to IR from human body may also enable the devices to be applied for the realization of artificial intelligence that contacts directly with human body such as artificial e-skin, biomedical monitoring, and tactile sensing.



## 1. Introduction

Transparent and flexible electronics (tf-electronics) devices that are lightweight, unbreakable, optically transparent, mechanically flexible and have a low power consumption are of great interest for the development of new-concept systems, such as displays, human–machine interfaces, electronic artificial skin, and smart digital gadgets [1–6]. However, there are several obstacles to the realization of optically transparent and flexible devices on plastic substrates [7–11], which include the limitations on the maximum process temperatures due to the low glass transition temperatures (80–200 °C) of the plastic substrates and the limited transparency and flexibility of the component materials in the devices. Therefore, for the realization of device components compatible with tf-electronics, the development of materials, processes, and structural designs with low temperature processability and good mechanical flexibility is the key issue.

Recent studies have demonstrated the fabrication of tf-electronic devices using transparent conducting oxides, carbon nanotubes or graphene as the electrodes, transparent oxide semiconductors, oxide nanowires or single-walled carbon nanotubes as the channels, and transparent oxide insulators or polymers as the insulators [9,10,12–18]. All of these researches have focused on improvement of performance, optical transparency, and mechanically flexibility of devices. However, there have been no reports on organic tf-electronics devices which use intrinsically transparent, flexible and organic thin film materials directly formed on transparent and flexible plastic substrates without transfer printing. The performances of organic tf-electronics devices are limited by the restricted

* Corresponding author at: School of Advanced Materials Science and Engineering, Sungkyunkwan University (SKKU), Suwon, Kyunggi 440-746, Republic of Korea. Tel.: +82 31 290 7398; fax: +82 31 290 7410.
*E-mail address:* nelee@skku.edu (N.-E. Lee).

1566-1199/$ - see front matter © 2012 Elsevier B.V. All rights reserved.
doi:10.1016/j.orgel.2011.12.015

electronic properties of organic materials such as, for example, their low mobility, $\mu$, of around 1 $cm^2 V^{-1} s^{-1}$ for organic field-effect transistors (OFETs) [19–22], which is three orders of magnitude lower than the value of ~1000 $cm^2 V^{-1} s^{-1}$ for inorganic FETs [23]. However, organic tf-electronics devices based on organic materials can provide advantages in the area of sensing devices, because the electrical performance of the sensing elements is less important than that in other systems such as integrated circuits.

Among the envisaged applications of organic electronic devices, OFETs offer a great deal of promise for applications in physical, chemical, and biological sensors [24–26] because OFET-based sensors have many advantages over other types of sensors such as signal amplification, high sensitivity, ease of fabrication, and miniaturization for multisensory arrays. Some research groups have recently reported flexible pressure sensors for electronic skin (e-skin) applications, in which OFETs were used to read out the pressure data from sensor elements [6,27,28]. Natural human skin, however, is much more complex, because multiple stimuli including, touch, temperature, pressure, and strain are sensed simultaneously. To imitate the tactile sensibility of natural human skin, therefore, artificial e-skins having multi-modal sensing capability are required for systems applicable to various environments. A sensor matrix with multi-functionalities was developed by some research groups by attaching two elemental sensors to each sensor cell (pixel) [28,29]. In the case of a multi-modal sensing configuration with multiple individual sensors, however, the density of the sensor pixels can be limited and the fabrication process becomes very complicated and expensive. Therefore, the fabrication of a type of sensor with the capability of sensing more than two stimuli simultaneously in the same sensing device would provide an interesting solution to the problem of artificial e-skin.

In this report, we demonstrate for the first time tf-OFETs directly integrated with multi-functional gate insulating materials, which have the potential to provide multi-modal sensing capability in a single sensing device. The advantages of these devices include their simple structure, easy integration, and responsiveness to multiple physical stimuli.

The key component of our devices is a layer of the highly crystalline co-polymer, P(VDF-TrFE), integrated directly into tf-OFETs as a multi-functional gate dielectric layer with piezoelectricity and pyroelectricity. The multi-modal sensing capability of the devices was examined by measuring their IR light response during mechanical bending. The AC (alternating current) gate biasing method was used to separate the pyro- and piezoelectric responses of gate dielectric (P(VDF-TrFE)) to multi-stimuli from the changes of other electrical parameters including their effective field-effect channel mobility and capacitance in the tf-OFETs. Furthermore, the pyro- and piezoelectric responses of the gate dielectrics causing the modulation of the device output signal could be decoupled, which indicates the feasibility of the multi-modal sensing from a single sensing device. Interestingly, the devices were also highly responsive to IR radiation from the human body, which has not been observed in other devices. These tf-OFETs with highly sensitivity to IR combined with mechanical sensing capability could be suitable for artificial e-skin, biomedical monitoring, and tactile sensing applications.

## 2. Measurement methods

Before the application of the sensor devices for multi-stimuli sensing, the characteristics of the tf-OFET were measured under ambient conditions by using a semiconductor parameter analyzer (HP 42145B). The results are shown in Supporting Fig. S1. In our devices, because the sensing layer is a gate dielectric layer of a ferroelectric co-polymer (P(VDF-TrFE)), the sensing mechanism depends on the modulation of the remnant polarization inside P(VDF-TrFE), $P_r$. For the sake of convenience we define the equivalent voltage, $V_0$, corresponding to $P_r$, $P_r = \varepsilon_0 \varepsilon_r V_0/d$, where $\varepsilon_0$, $\varepsilon_r$, and $d$ are the vacuum permittivity, relative dielectric permittivity and the thickness of the gate dielectric, respectively [30]. In order to investigate the capability of multi-modal sensing of the tf-OFETs, we applied an electric field directly to both sides of the P(VDF-TrFE) gate dielectric to pole and build up $P_r$ inside the P(VDF-TrFE) gate dielectric. In this case, the pentacene semiconductor layer and gate electrode served as poling electrodes.

It should be noted that the sensing layer of (P(VDF-TrFE)) functioned directly as a gate dielectric layer in the tf-OFETs. The sensing mechanism of the device based on the direct pyroelectric and piezoelectric effect can be explained by the change of $P_r$ or $V_0$ under external stimuli (IR, mechanical strain, or stress) that modulates the source–drain read-out current, $I_{DS}$ (see Eq. (1)). In addition, the external stimuli also affect the interference parameters, such as the hole mobility of pentacene, PEDOT:PSS/pentacene contact resistance and capacitance of the gate dielectric, which interfere with the modulated $I_{DS}$ from the tf-OFETs. The AC gate biasing method, which was reported in our previous work [31], served as a good technique to differentiate the responses to the physical stimuli caused by pyroelectricity and piezoelectricity from the other electrical interference parameters. The mathematical equation for the AC gate biasing method is presented in Eq. (1) [31]. The mathematical transforms and meaning of the parameters in the equation are provided in the Supporting Equation:

$$I_{DS} = -\mu C \frac{W}{L} V_{G0} V_D \sin(2\pi f t) - \mu C \frac{W}{L} V_0 V_D \quad (1)$$

here, $V_0$ is the equivalent external gate bias of $P_r$, $V_D$ is drain voltage, $\mu$ is the effective field-effect channel mobility, $C$ is the capacitance of the gate dielectric layer, $V_{G0}$ and $f$ are the amplitude and frequency of the applied AC gate bias, and $W$ and $L$ are the width and length of the channel, respectively. We define and $I_{DS}^{amp} = -\mu C \frac{W}{L} V_{G0} V_D$, and $I_{DS}^{mean} = -\mu C \frac{W}{L} V_0 V_D$, and $V_0$ is associated with $P_r$ of P(VDF-TrFE). To separate the response to the physical stimuli caused by pyroelectricity and piezoelectricity from the other electrical device parameters, we take the ratio of

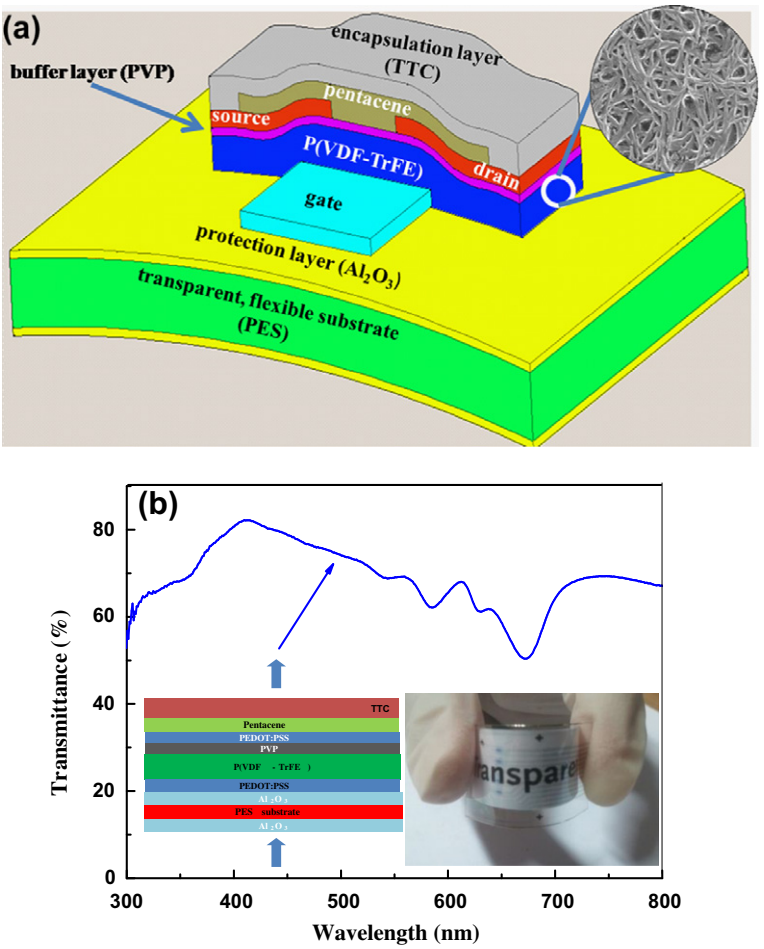


**Fig. 1.** The structure, optical image and transmittance of the tf-OFET. (a) Schematic illustration of tf-OFET. (b) Optical transmittance through all of the layers with the same stacking sequence and thickness as the layers in the tf-OFET device. The inset shows the image of a tf-OFET fabricated on a PES substrate with four devices, showing that the text on the paper behind the substrate is clearly visible.

$\frac{I_{DS}^{mean}}{I_{DS}^{amp}} = \frac{V_0}{V_{G0}}$ and then, from this ratio, we can calculate the response of $V_0$ or $P_r$ in the P(VDF-TrFE) copolymer.

## 3. Results and discussion

### 3.1. Optical transparency

To confirm the optical transmittance of devices, we measured optical transmission spectra through all of the stacked blanket layers on the transparent polyethersulfone (PES) substrate having the same thicknesses as those of the layers in the tf-OFET structure (see Fig. 1a). As shown in the results presented in Fig. 1b, the optical transmission of the sample with the stacked blanket layers on the PES substrate, with the substrate absorption eliminated, was about 70% in the visible wavelength range from 350 to 800 nm. The optical images of the tf-OFETs on the transparent and flexible substrate (see the inset in Fig. 1b) show transparency, in which the text on the paper behind the substrate with the devices is clearly visible.

### 3.2. Influence of IR irradiation

We investigated the IR response of the tf-OFETs by using the AC gate bias method. IR radiation from a halogen lamp acting as an IR source was focused on the device. A filter was placed in front of the halogen lamp to cut off all wavelengths shorter than 800 nm. When the device was illuminated with an IR light intensity of 2000 m W $cm^{-2}$, an increase in $I_{DS}$ was recorded at $V_D = -3$ V, $V_{G0} = -5$ V, and modulation frequency $f = 0.5$ Hz. The response data of $I_{DS}$ is shown in Fig. 2a. Such an increase of $I_{DS}$, including the augmentation of both $I_{DS}^{mean}$ and $I_{DS}^{amp}$ (Supporting Fig. S2 and Fig. 2b (green line)[1]), can be explained by the change in the effective mobility, due to the temperature dependence of the carrier transport in the pentacene layer, and the pyroelectric effect of the gate dielectric. When the tf-OFET is irradiated by IR at 20 °C to evaluate its multi-modal sensing capacity, the thermally

[1] For interpretation of color in Fig. 2, the reader is referred to the web version of this article.

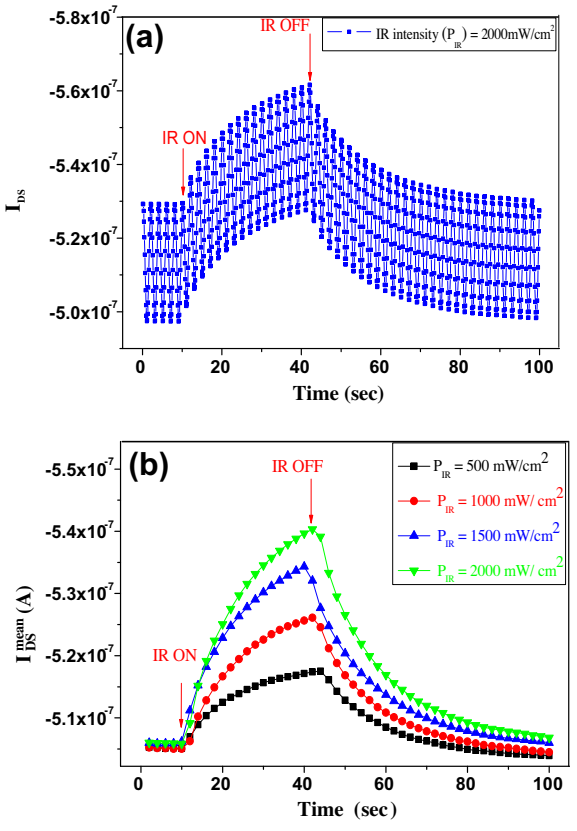


**Fig. 2.** Infrared response versus time for tf-OFET. (a) The infrared (IR) response of the device was measured by the AC gate biasing method. (b) Replotted response data of $I_{DS}^{mean}$ from the encapsulated device at various IR intensities.

activated hopping transport in pentacene is expected to be enhanced, where the hole mobility increases with increasing temperature following Arrhenius behaviour [32]. As a result, a net increase in $I_{DS}^{amp}$ and $I_{DS}^{mean}$ occurs, where $\mu$ is the multiplier factor in, $I_{DS}^{amp}$ and $I_{DS}^{mean}$ (see Eq. (1)). In addition, under IR illumination, the $V_0$ in the P(VDF-TrFE) gate dielectric also increases and so $I_{DS}^{mean}$ will increase, where $V_0$ is the multiplier factor in $I_{DS}^{mean}$ (see Eq. (1)). The increase of $V_0$ results from the positive pyroelectric response in the P(VDF-TrFE) gate dielectric. The positive pyroelectric phenomenon in the P(VDF-TrFE) gate dielectric will be discussed in more detail in relation to Fig. 3a. Fig. 2b presents the modulation of $I_{DS}^{mean}$ extracted from $I_{DS}$ at various IR light intensities (from 500 to 2000 m W cm$^{-2}$). The data show that the $I_{DS}^{mean}$ increases when IR light intensity increases.

### 3.3. Influence of physical multi-stimuli

As mentioned above, the AC gate biasing method can directly determine the pyroelectric and piezoelectric responses in multi-modal sensing devices. Therefore, we now study the capability of multi-stimuli sensing based on the modulation of $P_r$ or $V_0$ in P(VDF-TrFE) under IR, pressure, and strain applied separately. Fig. 3a shows the extracted $V_0$ values at different intensities of IR irradiation,

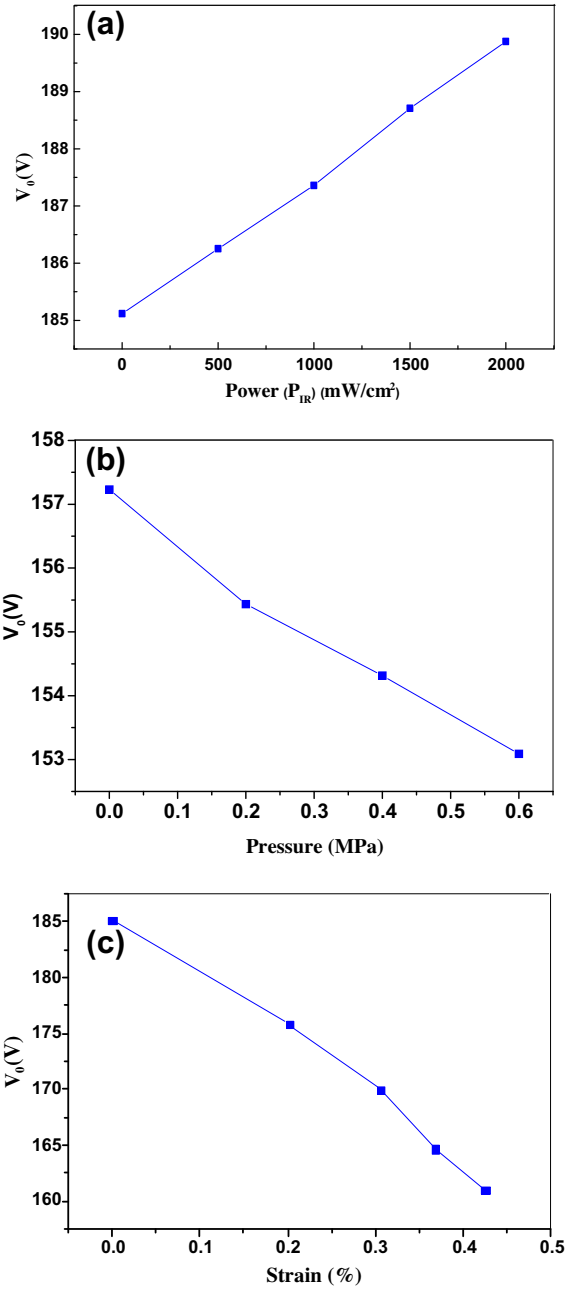


**Fig. 3.** Multi-stimuli responsiveness of tf-OFETs. (a) IR response of extracted $V_0$. (b) Pressure response of extracted $V_0$. (c) Strain response of extracted $V_0$.

$P_{IR}$. The results indicate a linear increase of $V_0$ with increasing $P_{IR}$. The increase of $V_0$ with increasing $P_{IR}$ indicates the positive pyroelectricity of P(VDF-TrFE). The pyroelectricity of P(VDF-TrFE) contains negative and positive contributions: the negative pyroelectricity proceeds from the thermal vibration of the dipoles in the amorphous phase (low crystallinity) at high temperature, which causes a reduction of the average dipole moment in the poling direction [30]. On the other hand, the positive pyroelectricity come from the thermal expansion of the crystals (high crystallin-

ity), which increases the dipole moments as the temperature increases [30]. Herein, we utilized highly crystalline β-phase P(VDF-TrFE), which leads to an increase in $P_r$ or $V_0$ as $P_{IR}$ increases, due to the thermal expansion of the crystalline phase. The phenomenon of the positive pyroelectricity of highly crystalline β-phase P(VDF-TrFE) in the temperature-sensitive device was also demonstrated in our previous work [30]. The mechanical sensitivity of the multi-modal sensing device was also examined. The plots in Fig. 3b and c show a decrease in the $V_0$ value with increasing compressive stress (pressure) and tensile strain (outward bending). The decrease of $V_0$ is attributed to the decreasing dipole density in P(VDF-TrFE) upon the application of compressive stress and tensile strain (outward bending) [31].

To investigate the multi-modal sensing capability in our device, responses of the device under simultaneous stimuli of IR irradiation and tensile strain were measured by exposing different IR irradiations at various tensile strains. The measured IR and tensile strain responses are illustrated in Fig. 4a and b, respectively. It can be seen that the responses to IR and tensile strain take place at the same time, and the IR sensitivity ($dV_0/dP_{IR}$) decreases from 0.0024 to 0.001 $Vm^{-1} W^{-1} cm^2$ with increasing tensile strain from 0% to 0.31%. The modulation in terms of $dV_0/dP_{IR}$ at various tensile strains is ascribed to the simultaneous pyroelectric and piezoelectric responses in the P(VDF-TrFE) gate dielectric. As mentioned above, the P(VDF-TrFE) in the device is the highly crystalline β-phase material, showing positive pyroelectricity, which leads to an increase in $P_r$ with increasing temperature or intensity of IR irradiation, due to the thermal expansion of the crystals. On the other hand, the dipoles in P(VDF-TrFE) will become less directional with increasing tensile strain, so $dV_0/dP_{IR}$ decreases at a high tensile strain.

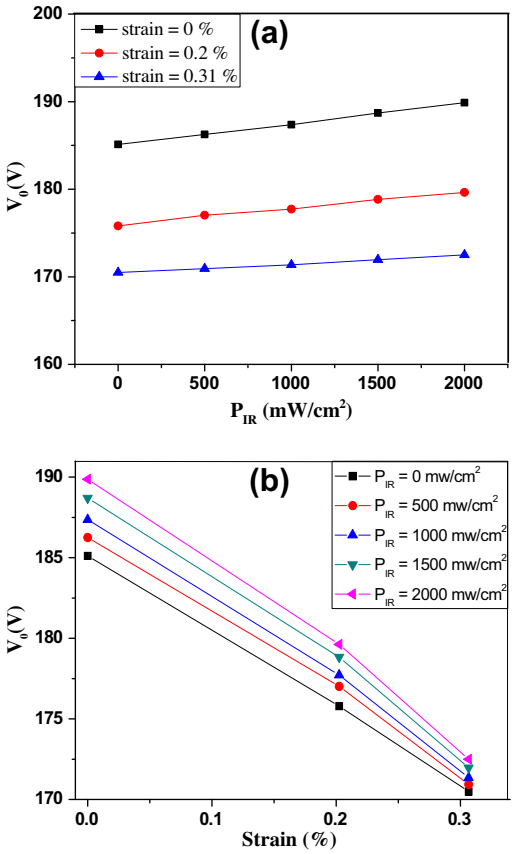


**Fig. 4.** Responses to simultaneous stimulation of IR irradiation and strain in tf-OFET. (a) The IR response of the extracted $V_0$ was measured at various strains. (b) The strain response of the extracted $V_0$ was measured at different IR power.

If we consider the modulation of $V_0$ only under simultaneous stimulation of IR exposure and strain in Fig. 4, we cannot make sure how the strain (piezoelectric response) or IR (pyroelectric response) makes an influence to the device. To decouple pyro- and piezoelectric responses quantitatively, we need more than one parameter of the devices contributing to modulation of the output signal. The term, $I_{DS}^{amp} = -\mu C \frac{W}{L} V_{G0} V_D$ obtained from AC gate biasing measurement method contains the contribution from the device parameters of $\mu$ and $C$ under simultaneous stimulation of IR and strain. Experimentally, the $C$ value did not change significantly because the change of $C$ is smaller 20 times compared to those of $\mu C$ under temperature or strain variation (no shown here). During measurements under multi-stimuli, the modulation in the $I_{DS}^{amp}$ can be affected not only by intrinsic channel mobility but also by other device parameter such as contact resistance $R_C$. In this case, the measured $\mu C$ values are not intrinsic values of the device but effective values, as defined in Eq. (1). The $\mu C$ values versus IR power and strain simultaneously are presented in the Supporting Fig. S3a and b. The increase of $\mu C$ values is presumably attributed to thermoresisitvity and piezoresistivity effects of pentacene under simultaneous stimulations of IR and strain, respectively. The responses of the device to two stimuli are decoupled by estimating the differences of two modulations; $V_0$ and $\mu C$ versus two input parameters (IR power and strain). Once $V_0$ and $\mu C$ at unknown value of two stimuli are determined, we can determine the input values of strain and IR power. The more details of decoupling process are explained together with the data in Supporting Fig. S4.

### 3.4. Study of repetitive mechanical deformation

For reliability evaluation of tf-OFETs under repetitive mechanical deformation, the sensing capability of the device was evaluated. To examine any change in the sensing capability of the device after repetitive mechanical bending with different bending cycles, $\frac{\Delta V_{0,IR\ or\ pr}}{\Delta V_{0,IR\ or\ pr}^{init}}$ values ($\Delta V_{0,IR\ or\ pr}^{init}$: the modulation of $V_0$ under IR or pressure at various bending cycles ($\Delta V_{0,IR\ or\ pr}^{init}$: the modulation of $V_0$ under IR or pressure without cyclic bending) under IR exposure (1000 m W $cm^{-2}$) and pressure (0.4 MPa) were monitored after the device is cyclically bent with bending cycles of 100, 1000, and 10,000 times at the bending radii of 1 cm (strain = 0.6%) and 1.5 cm (strain = 0.4%). Fig. 5a and b show the decrease in sensing capability in both IR and pressure responses. We recognize that the decrease

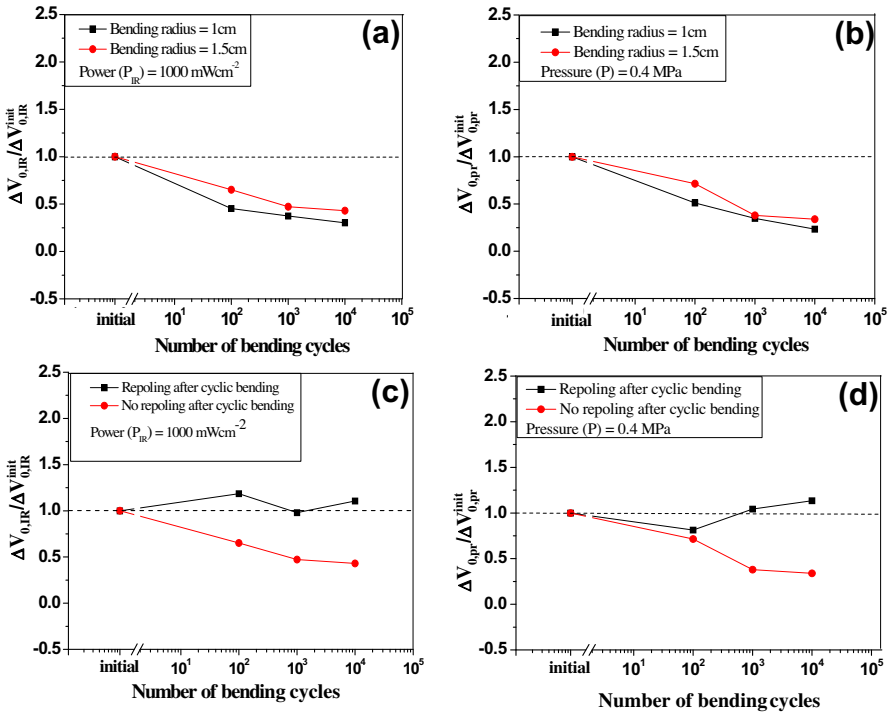


**Fig. 5.** IR and pressure sensing capability of the tf-OFET devices after various bending cycles at different bending radii was presented by $\frac{\Delta V_{0,IR\ or\ pr}}{\Delta V^{init}_{0,IR\ or\ pr}}$ value ($\Delta V_{0,IR\ or\ pr}$: the modulation of $V_0$ under IR or pressure at various bending cycles, $\Delta V^{init}_{0,IR\ or\ pr}$: the modulation of $V_0$ under IR or pressure without cyclic bending). (a and b) Sensing capability of the device under IR exposure and pressure, respectively, was measured at different bending radii (1 and 1.5 cm) and number of cyclic bending (100, 1000, and 10,000 cycles). (c and d) Sensing capability of the device under IR exposure and pressure, respectively, with and without re-poling was measured under the bending cycle number of 100, 1000, and 10,000 times at the bending radius of 1.5 cm.

in sensing capability of the device with the bending radius of 1 cm is larger than that of the device with the bending radius of 1.5 cm. The degradation in the sensing capability might be caused by disorder of dipole moment orientation induced inside the P(VDF-TrFE) dielectric layer leading to a decrease in $V_0$ (see Supporting Fig. S5) after cyclic bending. To enhance reordering of the orientation of dipole moments, the device was re-poled after bending cycles of 100, 1000, and 10,000 times at the bending radius of 1.5 cm. The Fig. 5c and d indicate that the $\frac{\Delta V_{0,IR\ or\ pr}}{\Delta V^{init}_{0,IR\ or\ pr}}$ values of the re-poled devices after bending cycles of 100, 1000, and 10,000 times is nearly unchanged compared to that of the device at the initial state before cyclic bending. From above results, we can presume that sensing capability of re-poled devices after cyclic bending is nearly stable.

### 3.5. Response to human body IR

Interestingly, the tf-OFET is highly responsive to IR radiation from the human body. The IR absorption spectrum of P(VDF-TrFE) (Supporting Fig. S6) shows absorption peaks in the wavelength range from 8000 to 9500 nm and from 11,000 to 12,000 nm. According to the thermal radiation theory at the temperature of the human body (300 K), the emitted wavelength ranges from 3000 to 70,000 nm, and the application of Wien's Law to the emission from the human body results in a peak wavelength of $\lambda_{peak} = 9500$ nm. From the above attributes of the IR absorption of P(VDF-TrFE) and human body radiation, we found that the wavelength of the bond or group variations in the P(VDF-TrFE) molecules matches with the IR wavelength range of the radiation from the human body. Consequently, P(VDF-TrFE) is expected to absorb the IR radiation from the human body efficiently. The response of the device to IR radiation from the human body was examined through the interaction between the devices and the human finger. When the finger is placed close to the device, heat transfer occurs from the finger to the device kept at 20 °C via conduction, convection and radiation. To vanish the effects of heat convection and conduction, we capped the finger with the polymer gloves, which is a heat insulator and transparent to IR. Here, the response of the devices was also measured by the AC gate biasing method, and $I^{mean}_{DS}$ extracted from the AC gate biasing method was determined as the current response to IR emitted from the human body.

Fig. 6a shows the series of data for the modulation of $I^{mean}_{DS}$ ($\Delta I^{mean}_{DS}$) as a function of the distance between the device and the finger, $d$, without and with bending. The augmentation of $I^{mean}_{DS}$ with decreasing $d$ can be explained by the variation in the intensity of the IR radiation with the change in $d$. When the intensity of the IR radiation is higher (i.e. $d$ decreases), more IR is absorbed by the P(VDF-TrFE) gate dielectric and, in turn, the existence of more dipole moments means that a higher $P_r$ or $V_0$ (positive pyroelectricity) is generated. Therefore, a greater number of holes are

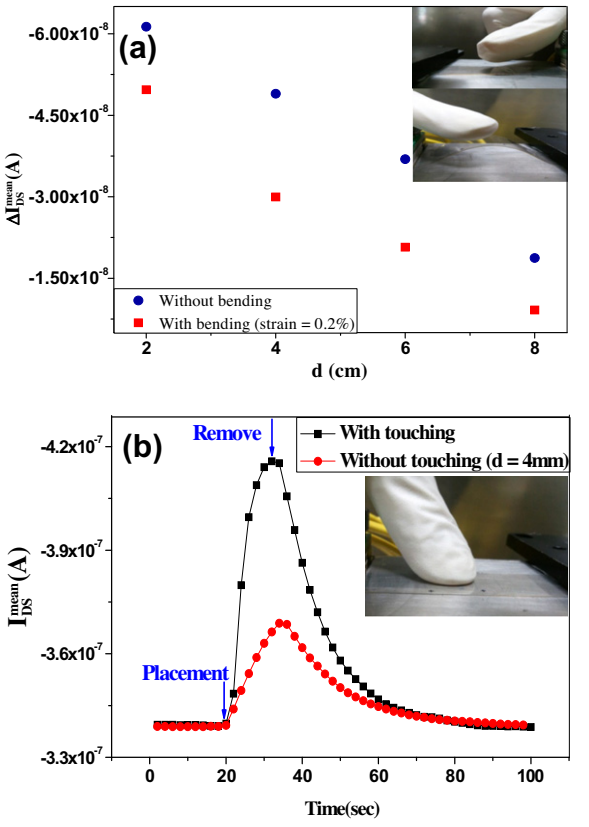


**Fig. 6.** Response of tf-OFET to IR from human body (finger). (a) The $I_{DS}^{mean}$ modulation of the tf-OFET without and with bending (strain = 0.2%) was measured at different distances, $d$, between the device and the finger. The inset image illustrates the measuring process. (b) The response of the device with and without finger touch (the finger was placed closely to the device with the distance of $d = 4$ mm). The inset image illustrates the measurement process.

trapped at the interface of pentacene/P(VDF-TrFE), generating a larger $\Delta I_{DS}^{mean}$. On the other hand, when the intensity of the IR radiation from the finger increases because the finger is closer to the surface of the device, a smaller $\Delta I_{DS}^{mean}$ is generated. In addition, this increase of $\Delta I_{DS}^{mean}$ is also related to the thermal effect on $\mu$ of pentacene. It is known that the electrical conductivity of semiconductor materials is usually thermally activated and therefore, under IR radiation, the holes mobility in pentacene increases with increasing intensity of IR radiation. Fig. 6b shows the response of the device to gentle finger touch. In this case, we placed the finger in contact with the device surface so that the touching force is very light. This means the signal response of the device mainly comes from IR response without pressure or strain response. The observed increase in $I_{DS}^{mean}$ is mainly caused by the thermal effect on $\mu$ of pentacene and the pyroelectric response of P(VDF-TrFE), due to the absorption of IR radiation from the finger. The results here demonstrate that the all-organic tf-FETs developed in this study, which are highly responsive to IR radiation from the human body, have a great potential in applications of biomedical monitoring and tactile sensing.

## 4. Conclusions

In this article, we report tf-OFETs with multi-modal sensing capability on transparent and flexible substrates. The highly crystalline co-polymer, P(VDF-TrFE), integrated directly into the tf-OFET makes it responsive to multiple external stimuli (viz. IR, pressure, and strain) with a simple and single device structure. The clear separation of the piezoelectric and pyroelectric responses from the other parameters was demonstrated by the AC gate biasing method. The present tf-OFETs devices with the capability of sensitively detecting IR radiation from the human body offer the promise of many interesting applications including, for example, biomedical monitoring and tactile sensing. In addition, the multi-modal sensing capability and simple fabrication of the FETs, based on organic, transparent and flexible materials, make them a promising candidate for artificial e-skin applications.

## 5. Experimental section

Tf-OFET sensing devices were fabricated in a bottom-gate and bottom-contact configuration on transparent PES substrate. The PES substrate has a high melting temperature of >200 °C with a thickness of 200 μm. The 20-nm-thick $Al_2O_3$ protection layers covering both sides of the PES substrate were deposited by atom layer deposition (ALD). The $Al_2O_3$ protective layers prevent the PES substrate from reacting with the organic solvent during the fabrication process. The spin-coated poly(3,4-ethylenedioxythiophene) poly(4-styrenesulfonate) (PEDOT:PSS), which was used as the gate, source and drain electrodes, was patterned by an $O_2$ CDE (chemical dry etching) process. After the spin-coating of PEDOT:PSS on the PES substrate, a thin film of Ni (5 nm) was deposited as an etch mask through a shadow mask onto the PEDOT:PSS film by e-beam evaporation. Then, the substrate was exposed to an oxygen microwave plasma in a CDE system at 640 mtorr and a microwave power of 50 W to etch the PEDOT:PSS which was not protected by the Ni patterns. Finally, the Ni mask patterns were removed in $HNO_3$ acid solution. With this patterning technique, tf-OFETs having a channel length ranging from 40 to 70 μm were obtained. The gate dielectric layer as a multi-stimuli responsive layer was formed by spin-coating P(VDF-TrFE) solution, subsequent melting at 200 °C for 1 h and annealing in a nitrogen medium at 140 °C for 2 h to increase the crystallinity for the enhancement of the piezoelectric and pyroelectric properties. Because the P(VDF-TrFE) used as a gate dielectric layer is a hydrophobic material, the PEDOT:PSS layer could not be spin-coated uniformly on the gate dielectric. To overcome this problem, a thin buffer layer of poly-4-vinyl phenol (PVP) (20 nm) between the dielectric and source/drain electrode was used. The hydrophilic surface of the PVP buffer layer was created by oxygen plasma treatment for the sequential formation of the gate dielectric and source/drain electrode. To minimize the degradation of the pentacene active layer during the electrical measurement with mechanical bending, a thin encapsulation layer of TTC (tetratetracontate) was capped on top of

the tf-OFET by thermal evaporation. The capping layer is also transparent to IR radiation.

## Acknowledgments

This research was supported by the Basic Science Research Program (Grant Nos. 2008-000-20533-0, 2010-0015035) and the WCU Program (Grant Nos. R32-2008-000-10124-0) through the National Research Foundation of Korea (NRF), funded by the Ministry of Education, Science and Technology (MEST), Republic of Korea.

## Appendix A. Supplementary data

Supplementary data associated with this article can be found, in the online version, at doi:10.1016/j.orgel.2011.12.015.

## References

[1] H.E.A. Huitema, G.H. Gelinck, J. van der Putten, K.E. Kuijk, C.M. Hart, E. Cantatore, P.T. Herwig, A. van Breemen, D.M. de Leeuw, Nature 414 (2001) 599.
[2] J.F. Wager, Science 300 (2003) 1245.
[3] G. Thomas, Nature 389 (1997) 907.
[4] S.R. Forrest, Nature 428 (2004) 911.
[5] R.H. Reuss, B.R. Chalamala, A. Moussessian, M.G. Kane, A. Kumar, D.C. Zhang, J.A. Rogers, M. Hatalis, D. Temple, G. Moddel, B.J. Eliasson, M.J. Estes, J. Kunze, E.S. Handy, E.S. Harmon, D.B. Salzman, J.M. Woodall, M.A. Alam, J.Y. Murthy, S.C. Jacobsen, M. Olivier, D. Markus, P.M. Campbell, E. Snow, Proc. IEEE 93 (2005) 1239.
[6] T. Someya, T. Sekitani, S. Iba, Y. Kato, H. Kawaguchi, T. Sakurai, Proc. Natl. Acad. Sci. USA 101 (2004) 9966.
[7] E.M.C. Fortunato, P.M.C. Barquinha, A. Pimentel, A.M.F. Goncalves, A.J.S. Marques, L.M.N. Pereira, R.F.P. Martins, Adv. Mater. 17 (2005) 590.
[8] L. Wang, M.H. Yoon, A. Facchetti, T.J. Marks, Adv. Mater. 19 (2007) 3252.
[9] J. Liu, D.B. Buchholz, J.W. Hennek, R.P.H. Chang, A. Facchetti, T.J. Marks, J. Am. Chem. Soc. 132 (2010) 11934.
[10] K. Nomura, H. Ohta, A. Takagi, T. Kamiya, M. Hirano, H. Hosono, Nature 432 (2004) 488.
[11] J. Liu, D.B. Buchholz, R.P.H. Chang, A. Facchetti, T.J. Marks, Adv. Mater. 22 (2010) 2333.
[12] S. Ju, A. Facchetti, Y. Xuan, J. Liu, F. Ishikawa, P. Ye, C. Zhou, T.J. Marks, D.B. Janes, Nature Nanotech. 2 (2007) 378.
[13] W.F. Zhang, Z.B. He, G.D. Yuan, J.S. Jie, L.B. Luo, X.J. Zhang, Z.H. Chen, C.S. Lee, W.J. Zhang, S.T. Lee, Appl. Phys. Lett. 94 (2009) 123103.
[14] S. Kim, S. Kim, J. Park, S. Ju, S. Mohammadi, ACSnano 4 (2010) 2994.
[15] T. Takenobu, T. Takahashi, Appl. Phys. Lett. 88 (2006) 033511.
[16] F.N. Ishikawa, H.K. Chang, K. Ryu, P.C. Chen, A. Badmaev, L.G.D. Arco, G. Shen, C. Zhou, ACSnano 3 (2009) 73.
[17] E. Artukovic, M. Kaempgen, D.S. Hecht, S. Roth, G. Gruner, Nano Lett. 5 (2005) 757.
[18] W.H. Lee, J. Park, S.H. Sim, S.B. Jo, K.S. Kim, B.H. Hong, K. Cho, Adv. Mater. 23 (2011) 1752.
[19] J. Zhang, Y. Zhao, Z. Wei, Y. Sun, Y. He, C. Di, W. Xu, W. Hu, Y. Liu, D. Zhu, Adv. Funct. Mater. 21 (2011) 786.
[20] A.L. Briseno, R.J. Tseng, M.M. Ling, E.H.L. Falcao, Y. Yang, F. Wudl, Z. Bao, Adv. Mater. 18 (2006) 2320.
[21] Y. Chen, Y. Xu, K. Zhao, X. Wan, J. Deng, W. Yan, Nano Res. 3 (2010) 714.
[22] K.J. Baeg, D.Y. Khim, J.H. Kim, M. Kang, I.K. You, D.Y. Kim, Y.Y. Noh, Org. Electron. 12 (2011) 634.
[23] J.P. Colinge, C.A. Colinge, Physics of Semiconductor Devices, Kluwer Academic, Boston, 2002.
[24] T.N.T. Nguyen, Y.G. Seol, N.-E. Lee, Org. Electron. 12 (2011) 1815.
[25] J.T. Mabeck, G.G. Malliaras, Anal. Bioanal. Chem. 384 (2006) 343.
[26] T. Someya, A. Dodabalapur, J. Huang, K.C. See, H.E. Katz, Adv. Mater. 22 (2010) 3799.
[27] S.C.B. Mannsfeld, B.C-K. Tee, R.M. Stoltenberg, C.V.H-H. Chen, S. Barman, B.V.O. Muir, A.N. Sokolov, C. Reese, Z. Bao, Nature Mater. 9 (2010) 859.
[28] T. Someya, Y. Kato, T. Sekitani, S. Iba, Y. Noguchi, Y. Murase, H. Kawaguchi, T. Sakurai, Proc. Nat. Acad. Sci. USA 102 (2005) 12321.
[29] I. Graz, M. Krause, S. Bauer-Gogonea, S. Bauer, S.P. Lacour, B. Ploss, M. Zirkl, B. Stadlober, S. Wagner, J. Appl. Phys. 106 (2009) 034503.
[30] N.T. Tien, Y.G. Seol, L.H.A. Dao, H.Y. Noh, N.E. Lee, Adv. Mater. 21 (2009) 910.
[31] N.T. Tien, T.Q. Trung, Y.G. Seol, D. Kim, N.E. Lee, ACSnano 5 (2011) 7069.
[32] D. Guo, T. Miyadera, S. Ikeda, T. Shimada, K. Saiki, J. Appl. Phys. 102 (2007) 023706.